Strong Asymmetric Charge Carrier Dependence in Inelastic Electron Tunneling Spectroscopy of Graphene Phonons

Fabian D. Natterer, Yue Zhao, Jonathan Wyrick, Yang-Hao Chan, Wen-Ying Ruan, Mei-Yin Chou, Kenji Watanabe, Takashi Taniguchi, Nikolai B. Zhitenev, and Joseph A. Stroscio

Phys. Rev. Lett. **114**, 245502 — Published 16 June 2015

DOI: 10.1103/PhysRevLett.114.245502

Strong Asymmetric Charge Carrier Dependence in Inelastic Electron Tunneling Spectroscopy of Graphene Phonons

Fabian D. Natterer[1†], Yue Zhao[1, 2†], Jonathan Wyrick[1†], Yang-Hao Chan[3], Wen-Ying Ruan[4], Mei-Yin Chou[3,4], Kenji Watanabe[5], Takashi Taniguchi[5], Nikolai B. Zhitenev[1*], and Joseph A. Stroscio[1,*]

[1]Center for Nanoscale Science and Technology, National Institute of Standards and Technology, Gaithersburg, MD 20899, USA
[2]Maryland NanoCenter, University of Maryland, College Park, MD 20742, USA
[3]Institute of Atomic and Molecular Sciences, Academia Sinica, Taipei 10617, Taiwan
[4]School of Physics, Georgia Institute of Technology, Atlanta, GA 30332, USA
[5]Advanced Materials Laboratory, National Institute for Materials Science, Tsukuba, Ibaraki 305-0044 JAPAN
†These authors contributed equally to this work

Abstract:

The observation of phonons in graphene by inelastic electron tunneling spectroscopy has been met with limited success in previous measurements arising from weak signals and other spectral features which inhibit a clear distinction between phonons and miscellaneous excitations. Utilizing a back gated graphene device that allows adjusting the global charge carrier density, we introduce an averaging method where individual tunneling spectra at varying charge carrier density are combined into one representative spectrum. This method improves the signal for inelastic transitions while it suppresses dispersive spectral features. We thereby map the total graphene phonon density of states, in good agreement with density functional calculations. Unexpectedly, an abrupt change in the phonon intensity is observed when the graphene charge carrier type is switched through a variation of the back gate electrode potential. This sudden variation in phonon intensity is asymmetric in carrier type, depending on the sign of the tunneling bias.

* To whom correspondence should be addressed: nikolai.zhitenev@nist.gov, joseph.stroscio@nist.gov

Phonons are the fundamental vibrational modes of a crystal lattice. They play a major role in many physical properties related to thermal and electrical conductivities, such as heat capacity, electrical resistance, lattice deformations etc. In graphene, phonons participate in the renormalization of the Fermi velocity due to electron-phonon coupling and many-body interactions [1]. Phonons are the main mechanism for energy dissipation and are critical to the understanding and control of promising new electron and optical graphene-based devices [2–4]. Many techniques have been applied to measure graphene and graphite phonons, including neutron scattering [5], x-ray scattering [6], Raman spectroscopy [7–9], electron energy-loss spectroscopy [10], and inelastic electron tunneling spectroscopy (IETS) [11–16].

The ability to detect phonons has been very important in many graphene applications. This has led, for example, to the routine application of Raman spectroscopy to graphene physics and devices [9]. IETS detects vibrational excitations without the stringent selection rules active in Raman spectroscopy [17], and it's employment in a scanning tunneling microscope (STM) brings about spatial mapping of inelastic processes [18]. Inelastic excitations appear in scanning tunneling spectroscopy as a set of steps in the differential tunneling conductance at the excitation energy $\varepsilon = \hbar\omega$, and as a peak and dip pair at positive and negative sample biases, $\pm\varepsilon$, in the second derivative [18]. Previously, IETS has had limited success in measuring phonons in graphene because of weak signals and spectral overlap with other miscellaneous excitations. To date only a few reports of phonons in graphene have been published [13–16]. Reference [13] characterized an excitation at 63 meV and assigned it to a *K*-point phonon, while reference [14] revealed an additional feature at 150 meV and also assigned it to a *K*-point phonon. Reference [15] detected an excitation at 360 meV, which was tentatively assigned to a breathing mode.

In this letter, we show that careful measurements utilizing a back gated graphene device, where the graphene charge carrier density can be varied in magnitude and sign, allows all graphene excitations with appreciable density of states (DOS) to be observed by IETS, in good agreement with density functional theory (DFT) calculations [19]. In total we observe five excitations from phonons near the Γ, *M*, and *K* points in the surface Brillouin zone and one additional overtone mode, which are summarized in Table 1. More importantly, we find that all six excitations are strongly dependent on the graphene charge carrier type, with a large step-like change in intensity when the carrier type is switched by sweeping the back gate voltage of the graphene device. We notice a concurrence of this change in phonon intensity with the presence of quasi-bound state resonances induced by the tip potential [20] and thus consider the involvement of these states in a resonant inelastic excitation process, in analogy to resonant excitations involving molecular systems on surfaces [21–24].

A field effect device, consisting of a graphene layer on top of hexagonal boron nitride (*h*-BN) on SiO_2 with a doped Si back gate, was fabricated using a dry transfer technique [25] and followed by e-beam lithography to deposit Au contacts [19]. Measurements were performed with a custom-built low temperature STM, operating at 4.3 K and a base pressure better than 5×10^{-11} hPa [26,27]. All phonons were observed in repeated measurements, independent of sample location, and were unperturbed by the exposure of graphene to molecular hydrogen and deuterium. The latter gases were used to rule out false assignment of the observed features to background gas or contamination from device fabrication processes [24,28,29]. The graphene topography images showed perfect lattices without contamination, as in previous studies [30]. In a technique referred to as gate-mapping tunneling spectroscopy [30,31], the differential conductance (*dI/dV*) was recorded as a function of tunneling sample bias, V_b, and gate voltage,

V_g, by adding a sinusoidal voltage with root-mean-square amplitude in the range of (4 to 10) mV to the sample bias at 203.5 Hz; both dI/dV and d^2I/dV^2 signals were detected simultaneously with a dual-harmonic lock-in amplifier using individually optimized phases and a time constant, τ, in the range of (0.1 to 1) s. The second derivative signal, d^2I/dV^2, is referred to as the IETS signal.

For the present work we employ a mapping method [32], referred to as gate-averaged spectroscopy, where we calculate the average of all spectra that were recorded over our full gate voltage range. The advantage of gate-averaged spectroscopy becomes evident when noting there are a plethora of states probed with scanning tunneling spectroscopy in graphene, for instance due to scattering resonances or surface plasmons. Many of these excitations delicately depend on the charge carrier density and will consequently appear at different energies for different doping levels (here controlled by V_g), while inelastic excitations show up at their characteristic threshold energy $\pm\hbar\omega$ [33]. Figure 1 illustrates the result of gate-voltage-averaged spectroscopy for single-layer graphene on *h*-BN/SiO_2. We recorded gate-voltage-averaged *dI/dV* [Fig. 1(a)] and IETS [Fig. 1(b)-(e)] with the technique described above. Six excitations can be resolved as small steps in *dI/dV* showing a change in differential conductance of about 5 % on average. These excitations are better discerned in IETS, where they appear as point symmetric peaks ($+\hbar\omega_{1-6}$) and dips ($-\hbar\omega_{1-6}$) with respect to zero bias. The latter identifies them as inelastic excitations. We obtain a precise measure of the transition energies $\hbar\omega_{1-6}$, summarized in Table 1, by focusing on energy windows around the various thresholds with sets of separate gate-averaged measurements using longer averaging times [Fig. 1(c)-(e)].

A comparison with literature [6] and supporting DFT calculations [Fig. 2] shows the excellent agreement for $\hbar\omega_{1-5}$ with phonons from the high symmetry points in the graphene

Brillouin zone. The dashed ribbons in Fig. 2(b) indicate the overlap between the measured excitations and the calculated phonon DOS. The associated dispersion relation in Fig. 2(a) reveals that the first four maxima are due to a series of van-Hove singularities at the *M* point. In addition, a ring of phonon energy maxima centered at Γ in the Brillouin zone exists near 200 meV, giving rise to the last high energy peak in the calculated DOS. Following the notation in Ref. [6], we attribute the two low lying modes $\hbar\omega_{1,2}$ to out-of-plane phonons (M_{3+}, $M_{2\pm}$) which were previously ascribed to a single *K* phonon [13,14]. A closer examination of the data in Ref. [13] shows a splitting of the 63 meV transition into two separate excitations, similar to what is seen in our work in Fig. 1(c) [19]. The mode $\hbar\omega_3$ is close in energy to the K_5 phonon and appears with comparable intensity in our IETS data with the nearby $\hbar\omega_4$ and $\hbar\omega_5$ modes, despite only a small maximum in the phonon DOS near this energy. This may be explained by the fact that a *K* phonon can provide the right momentum to scatter a Dirac electron from one valley to another. Phonon $\hbar\omega_4$ can be related to a normal mode with symmetry M_{3-} that is a saddle point. The mode $\hbar\omega_5$ can be attributed to the Γ_{5+} mode, which is known to have a strong electron-phonon interaction, or the last peak in the DOS arising from a ring of energy maxima around Γ in the phonon spectra.

The assignment of the high energy transition $\hbar\omega_6$ is more complex, since it lies well above the topmost graphene phonon band. In Raman spectroscopy of graphene, the strongest signal derives from a high energy overtone mode, the 2D peak at ≈335 meV [7]. This mode energy is too far off the observed $\hbar\omega_6$ mode at 359 meV in Fig. 1, suggesting a different origin of the $\hbar\omega_6$ transition. In the following we will propose that this excitation is possibility related to other overtones of graphene phonons. We tentatively attribute this mode to the simultaneous emission of two phonons from Γ_5 and K_1 or from the ring of highest-energy phonons around Γ

and K_1. The combined calculated threshold lies at 356 meV ($\Gamma_5 + K_1$) or 361 meV (Γ ring + K_1), and is in better agreement with our observed excitation at (359 ± 1) meV [34]. We note that Γ_5 and K_1 have the largest electron-phonon interaction matrix elements in the calculation of the phonon self-energy and that K_1 is not observed directly in our spectrum but through a second order effect combined with Γ_5.

Our results show signatures of large parts of the graphene phonon DOS in our IETS data, irrespective of mode type or amplitude direction. Even more complex in the case of graphene is that there are only electronic states at the *K*-point in the Brillouin zone in the examined bias-voltage range. Therefore, only phonons near Γ and *K* will be involved with electron-phonon scattering processes in a perfect graphene sheet. Most previous investigations on the electron-phonon scattering in graphene have focused on these phonons. In contrast, our IETS measurements show the signature of inelastic scattering between Dirac particles through the coupling to all the various phonon modes. This finding requires relaxation of the crystal momentum conservation in our graphene device. This may result from a small lattice deformation or a variation of the external potential in the presence of the tunneling tip and the *h*-BN substrate layer that slightly breaks the perfect crystal symmetry. As shown in a previous theoretical calculation [35], any lattice deformation could induce band mixing between states at *K* and other parts of the Brillouin zone and lead to an enhancement of the tunneling DOS at various phonon thresholds. More recent first principles calculations have identified multiple excitations appearing in IETS, which are also sensitive to defects and adsorbates [36]. We note that our phonon measurements were reproduced at various spatial locations in graphene; however, direct investigation of defect sites was not attempted.

We now focus on a strong asymmetry selection rule observed in the gate-voltage-resolved spectroscopy. By invoking the just-established knowledge about the phonons $\hbar\omega_{1-6}$, we will illustrate how the phonon intensities strongly depend on the charge carrier type. Figure 3(a) shows an IETS gate map in the gate interval ±40 V and for a sample bias range of ±500 mV. The relevant features for the current discussion are the inelastic excitations that show up as horizontal lines at $\pm\hbar\omega$ in Figure 3(a) and (c), and how they relate to the tip induced quasi-bound states [20]. Mode $\hbar\omega_6$ is quite straightforward to discern, in contrast to excitations $\hbar\omega_{1-5}$. One may, however, with the knowledge established above, spot the latter phonons as faint horizontal lines, annotated by numbered arrows. The occurrence of such weak excitations stresses anew the value of the gate-voltage-averaged spectroscopy [Fig. 1]. When we take a closer look at the individual excitations in Fig. 3(a), we observe two notable asymmetries in the phonon intensities. The first concerns the asymmetry with respect to bias voltage: the phonon intensity is weak at $+\hbar\omega$ and strong at $-\hbar\omega$, for electron doping, as can best be seen for $\hbar\omega_6$ at a gate voltage of +40 V. The second asymmetry occurs with respect to gate voltage at constant threshold $\hbar\omega$. Figure 3(b) traces the gate dependent phonon intensity for the $\hbar\omega_6$ mode. It indicates an effectively binary transition with fivefold enhancement in the phonon intensity around a gate voltage of 0 V ($+\hbar\omega_6$) and -20 V ($-\hbar\omega_6$). The difference in gate voltage for the transitions is due to the tip gating effect that slants the charge neutrality axis in the gate map. Figure 3(c) shows an additional IETS measurement where the tip work function was deliberately increased. The electron-hole boundary was thereby shifted to the right, along with the onset of the high to low intensity transition of the $\hbar\omega_6$ mode (cf. Fig. 3(c)). Quite surprisingly an examination of our gate maps shows that all the observed phonons exhibit these asymmetries

with respect to charge carrier density and bias voltage, see Table 1. The determined enhancement ratios follow a linear trend in energy with a slope $(17 \pm 4)\ eV^{-1}$.

The data in Fig. 3 indicate that graphene phonons are resonantly enhanced when the graphene charge carrier is switched. While the back gate voltage is setting the global carrier density, the STM probe tip can locally increase or overturn the doping in the region below the tip apex. These competing trends in doping can result in the formation of local circular *pn* junctions for certain values of the gate map parameters, and yield quasi-bound state resonances resembling whispering gallery modes (WGM) for electrons and holes [20]. These WGM resonances are most noticeable as the "S" shaped interference fringes in the gate maps in Figs. 3, (a) and (c). In the resonant excitation process for tunneling electrons, an electron from the source is temporarily trapped in a resonance state before it relaxes inelastically towards the drain [22,23]. Invoking this picture, the quasi-bound WGM resonances would consequently mimic a "giant" molecule, the resonances acting as the intermediate state for the tunneling electrons. As long as the WGM resonance is available, an enhanced phonon intensity is observed. For example, the abrupt change in intensity at constant positive tunneling bias transpires when a switch in the charge carrier type from holes to electrons occurs, delineated by the "S" fan in Figs. 3 (a) and (c). This is the same point where the WGM resonances change occupancy, and are not available as an intermediate state. We therefore suggest that WGM resonances in the circular *pn* junctions can affect the phonon excitations in the same way as molecular states can give rise to resonant excitation of molecular- vibrational or rotational modes [21–24]. A detailed quantitative explanation of the carrier dependence of the phonon intensities for IETS awaits further theoretical work.

Acknowledgements

Y. Z. acknowledges support under the Cooperative Research Agreement between the University of Maryland and the National Institute of Standards and Technology Center for Nanoscale Science and Technology, Grant No. 70NANB10H193, through the University of Maryland. J.W. acknowledges support from the Nation Research Council Fellowship. F. D. N. greatly appreciates support from the Swiss National Science Foundation under project numbers 148891 and 158468. Theoretical work at Georgia Tech is supported by the U.S. Department of Energy, Office of Basic Energy Sciences, Division of Materials Sciences and Engineering under Award No. DEFG02−97ER45632. Y.-H. C. is supported by a Thematic Project at Academia Sinica. We thank Mark Stiles, Leonid Levitov, and Mats Persson for valuable discussions, and Steve Blankenship and Allan Band for their technical contributions to this project.

Table 1: Phonon threshold energies obtained from a series of IETS spectra, such as the ones shown in Fig. 1(b-e). Also listed are the calculated phonon energies at high symmetry points from density functional theory (DFT) that are close to the IETS threshold energies. The enhancement ratio (ER) describes the dependence of the phonon intensity with charge carrier density. The uncertainties are one standard deviation of the mean from the statistical distribution. The sample sizes N, for each measure is given in parentheses.

ħω	**IETS (meV)**	**DFT (meV)**	**Phonons**	**ER**
1	56.8 ± 0.9 (12)	58	M_{3+}	1.6 ± 0.6 (10)
2	80.9 ± 1.3 (12)	78	$M_{2\pm}$	1.9 ± 0.7 (10)
3	152.8 ± 1.2 (9)	149	K_5	4.3 ± 1.8 (6)
4	176.9 ± 1.5 (9)	173	M_{3-}	3.5 ± 1.0 (6)
5	195 ± 2 (9)	194 / 199	Γ_{5+} / Ring around Γ	7.1 ± 3.0 (6)
6	359 ± 1 (6)	356 / 361	$\Gamma_{5+} + K_1$ / Ring + K_1	5.8 ± 2.6 (17)

Figure Captions:

Figure 1: Phonon spectroscopy of single layer graphene on an *h*-BN/SiO_2 field effect device. The *dI/dV* spectra in (**a**) and d^2I/dV^2 data in (**b**-**e**) are the average of a series of spectra recorded over charge carrier concentrations, tuned by the back gate electrode from $V_g = -40$ V to $+40$ V. The inelastic transitions (1 to 5) are attributed to phonons in graphene and excitation (6) to an overtone. (**c**-**e**) Higher resolution portions of the d^2I/dV^2 spectra with increased averaging times. Symbols are experimental data, dashed lines show fits to single Lorentzian functions, and solid lines the sum of the fits, except the blue dashed line in (c) connecting data symbols. Peak numbers refer to excitations in Table 1. A linear background was subtracted from d^2I/dV^2 spectra in (b-e).

Figure 2: (**a**) Phonon dispersion and (**b**) phonon density of states (DOS) for single layer graphene obtained from density functional calculations. The observed phonon threshold energies are indicated by horizontal dashed lines with two experimentally determined standard deviations between lines.

Figure 3: Gate-voltage-dependent phonon spectroscopy of single layer graphene on *h*-BN/SiO_2. (**a**) d^2I/dV^2 gate map showing the asymmetry of the phonon intensity with sample tunneling bias, V_b and back gate voltage, V_g. The excitations $\hbar\omega_1$ to $\hbar\omega_6$ from Fig. 1 are indicated by the arrows. (**b**) d^2I/dV^2 data tracing the gate-dependent phonon intensity, using mode $\hbar\omega_6$ as an example. The peak height ratio between the outermost gate values around ±40 V is 8.1 ± 0.9 $(+\hbar\omega_6)$ and 7.3 ± 0.6 $(-\hbar\omega_6)$. The uncertainties were derived from the standard error of d^2I/dV^2values in the gate voltage range between ±(40 to 20) V. (**c**) d^2I/dV^2 gate map showing the asymmetry of the phonon excitations. The tip work function has been increased relatively to the measurement in (a) by adsorption of deuterium, resulting in a shift of the electron vs. hole boundary to positive gate voltages in the gate map [20]. The intervals enclosed by arrows denote the regions where the $\hbar\omega_6$ mode is enhanced.

References

[1] D. N. Basov, M. M. Fogler, A. Lanzara, F. Wang, and Y. Zhang, Rev. Mod. Phys. **86**, 959 (2014).
[2] R. Bistritzer and A. H. MacDonald, Phys. Rev. Lett. **102**, 206410 (2009).
[3] W.-K. Tse and S. Das Sarma, Phys. Rev. B **79**, 235406 (2009).
[4] M. W. Graham, S.-F. Shi, D. C. Ralph, J. Park, and P. L. McEuen, Nat. Phys. **9**, 103 (2013).
[5] R. Nicklow, N. Wakabayashi, and H. G. Smith, Phys. Rev. B **5**, 4951 (1972).
[6] M. Mohr, J. Maultzsch, E. Dobardžić, S. Reich, I. Milošević, M. Damnjanović, A. Bosak, M. Krisch, and C. Thomsen, Phys. Rev. B **76**, 035439 (2007).
[7] A. C. Ferrari, J. C. Meyer, V. Scardaci, C. Casiraghi, M. Lazzeri, F. Mauri, S. Piscanec, D. Jiang, K. S. Novoselov, S. Roth, and A. K. Geim, Phys. Rev. Lett. **97**, 187401 (2006).
[8] A. C. Ferrari, Solid State Commun. **143**, 47 (2007).
[9] L. M. Malard, M. A. Pimenta, G. Dresselhaus, and M. S. Dresselhaus, Phys. Rep. **473**, 51 (2009).
[10] S. Siebentritt, R. Pues, K.-H. Rieder, and A. M. Shikin, Phys. Rev. B **55**, 7927 (1997).
[11] D. P. E. Smith, G. Binnig, and C. F. Quate, Appl. Phys. Lett. **49**, 1641 (1986).
[12] L. Vitali, M. A. Schneider, K. Kern, L. Wirtz, and A. Rubio, Phys. Rev. B **69**, 121414 (2004).
[13] Y. Zhang, V. W. Brar, F. Wang, C. Girit, Y. Yayon, M. Panlasigui, A. Zettl, and M. F. Crommie, Nat. Phys. **4**, 627 (2008).
[14] V. W. Brar, S. Wickenburg, M. Panlasigui, C.-H. Park, T. O. Wehling, Y. Zhang, R. Decker, Ç. Girit, A. V. Balatsky, S. G. Louie, A. Zettl, and M. F. Crommie, Phys. Rev. Lett. **104**, 036805 (2010).
[15] A. Castellanos-Gomez, G. Rubio-Bollinger, S. Barja, M. Garnica, A. L. V. de Parga, R. Miranda, and N. Agraït, Appl. Phys. Lett. **102**, 063114 (2013).
[16] G. Li, A. Luican, and E. Y. Andrei, Phys. Rev. Lett. **102**, 176804 (2009).
[17] N. Lorente, M. Persson, L. J. Lauhon, and W. Ho, Phys. Rev. Lett. **86**, 2593 (2001).
[18] B. C. Stipe, M. A. Rezaei, and W. Ho, Science **280**, 1732 (1998).
[19] See Supplemental Material [url], which includes Refs. [37-45].
[20] Y. Zhao,, J. Wyrick, F. D. Natterer, J. F. Rodriguez-Nieva3, C. Lewandowski, K. Watanabe, T. Taniguchi, L. S. Levitov, N. B. Zhitenev, and J. A. Stroscio, Science **348**, 672 (2015).
[21] J. Gadzuk, Phys. Rev. B **31**, 6789 (1985).
[22] B. Persson and A. Baratoff, Phys. Rev. Lett. **59**, 339 (1987).
[23] A. Baratoff and B. N. J. Persson, J. Vac. Sci. Technol. A **6**, 331 (1988).
[24] F. D. Natterer, F. Patthey, and H. Brune, ACS Nano **8**, 7099 (2014).
[25] L. Wang, I. Meric, P. Y. Huang, Q. Gao, Y. Gao, H. Tran, T. Taniguchi, K. Watanabe, L. M. Campos, D. A. Muller, J. Guo, P. Kim, J. Hone, K. L. Shepard, and C. R. Dean, Science **342**, 614 (2013).
[26] J. A. Stroscio, E. W. Hudson, S. R. Blankenship, R. J. Celotta, and A. P. Fein, Proc. SPIE **4608**, 112 (2002).
[27] R. J. Celotta, S. B. Balakirsky, A. P. Fein, F. M. Hess, G. M. Rutter, and J. A. Stroscio, Rev. Sci. Instrum. **85**, 121301 (2014).
[28] F. D. Natterer, F. Patthey, and H. Brune, Phys. Rev. Lett. **111**, 175303 (2013).

[29] S. Li, A. Yu, F. Toledo, Z. Han, H. Wang, H. He, R. Wu, and W. Ho, Phys. Rev. Lett. **111**, 146102 (2013).
[30] J. Chae, S. Jung, A. F. Young, C. R. Dean, L. Wang, Y. Gao, K. Watanabe, T. Taniguchi, J. Hone, K. L. Shepard, P. Kim, N. B. Zhitenev, and J. A. Stroscio, Phys. Rev. Lett. **109**, 116802 (2012).
[31] S. Jung, G. M. Rutter, N. N. Klimov, D. B. Newell, I. Calizo, A. R. Hight-Walker, N. B. Zhitenev, and J. A. Stroscio, Nat Phys **7**, 245 (2011).
[32] C. E. Malec and D. Davidović, J. Appl. Phys. **109**, 064507 (2011).
[33] R. C. Jaklevic and J. Lambe, Phys. Rev. Lett. **17**, 1139 (1966).
[34] The uncertainty represents one standard deviation.
[35] T. O. Wehling, I. Grigorenko, A. I. Lichtenstein, and A. V. Balatsky, Phys. Rev. Lett. **101**, 216803 (2008).
[36] M. L. N. Palsgaard, N. P. Andersen, and M. Brandbyge, ArXiv14103001 Cond-Mat (2014).
[37] L. Wang, I. Meric, P. Y. Huang, Q. Gao, Y. Gao, H. Tran, T. Taniguchi, K. Watanabe, L. M. Campos, D. A. Muller, J. Guo, P. Kim, J. Hone, K. L. Shepard, and C. R. Dean, Science **342**, 614 (2013).
[38] Certain commercial equipment, instruments, or materials are identified in this paper in order to specify the experimental and theoretical procedures adequately. Such identification is not intended to imply recommendation or endorsement by the National Institute of Standards and Technology, nor is it intended to imply that the materials or equipment identified are necessarily the best available for the purpose.
[39] G. Kresse and J. Hafner, Phys. Rev. B **48**, 13115 (1993).
[40] G. Kresse and J. Furthmüller, Computational Materials Science **6**, 15 (1996).
[41] G. Kresse and J. Furthmüller, Phys. Rev. B **54**, 11169 (1996).
[42] P. E. Blöchl, Phys. Rev. B **50**, 17953 (1994).
[43] G. Kresse and D. Joubert, Phys. Rev. B **59**, 1758 (1999).
[44] J. P. Perdew, K. Burke, and M. Ernzerhof, Phys. Rev. Lett. **77**, 3865 (1996).
[45] A. Togo, F. Oba, and I. Tanaka, Phys. Rev. B **78**, 134106 (2008).

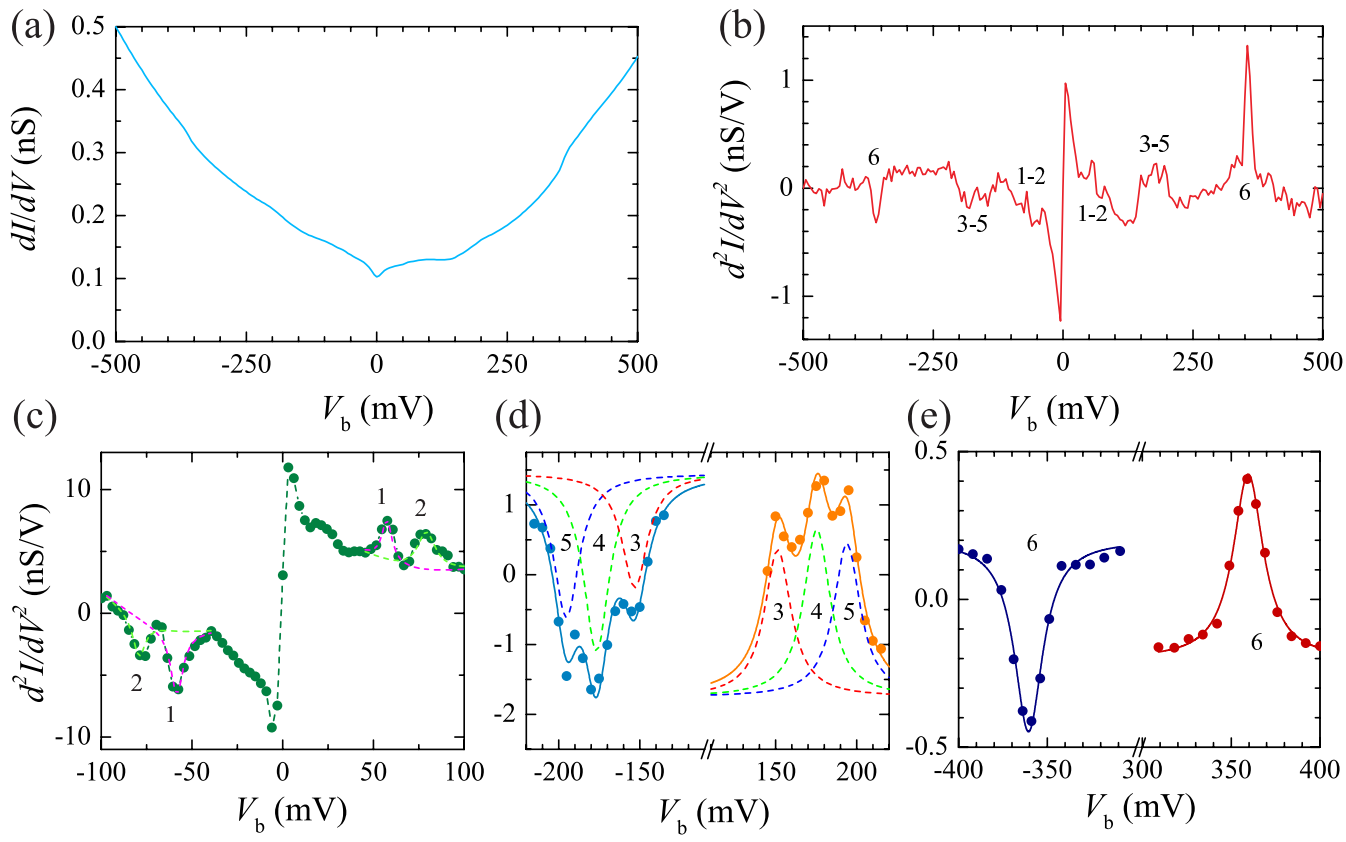

Figure 1: print full 3 columns

Figure 1 LB15177 20MAY2015

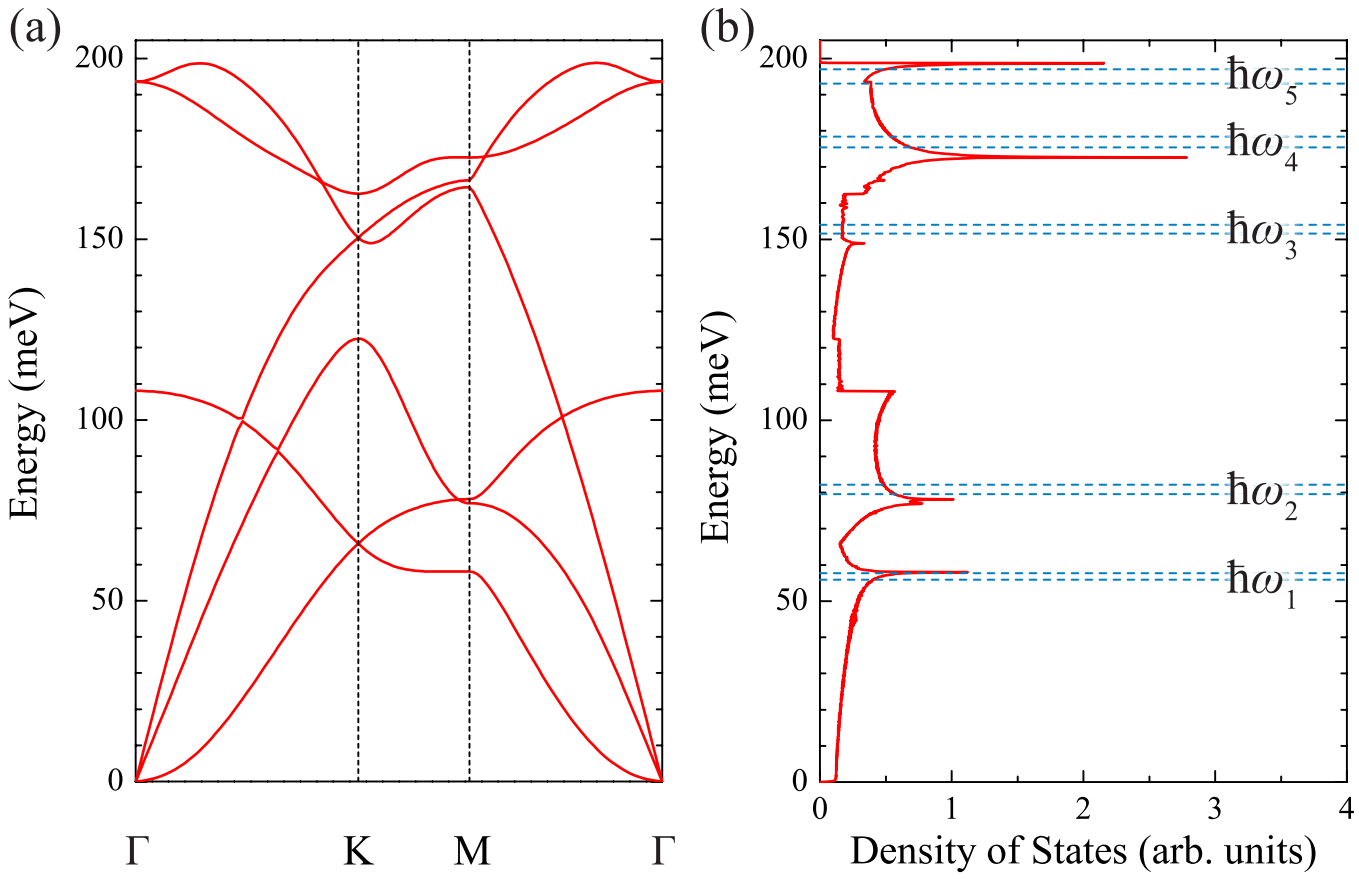

LB15177 updated Figure 2. Please print full single column wide.

Figure 2 LB15177 20MAY2015

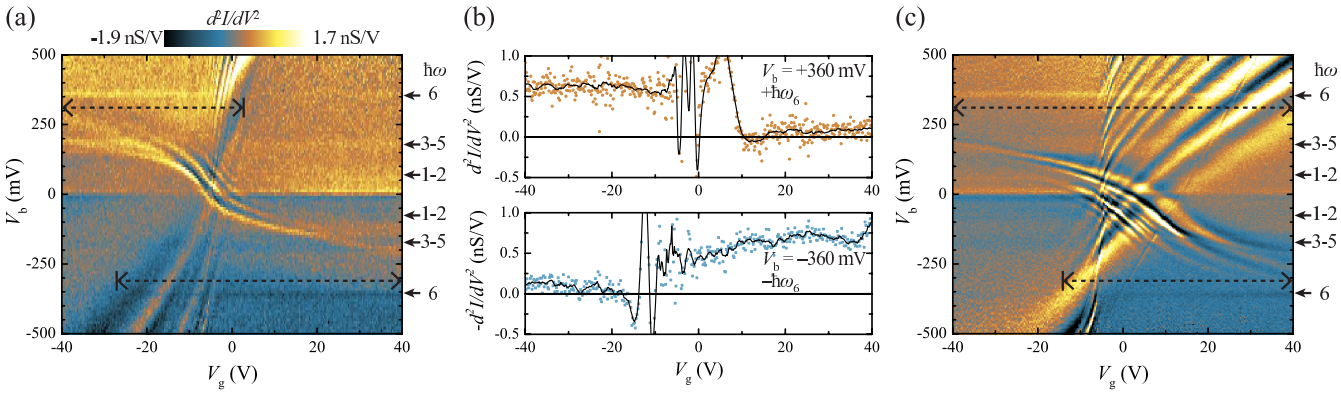

LB15177 updated Figure 3. Please print FULL double column wide.

Figure 3 LB15177 20MAY2015